



---

# Audio Engineering Society Convention Paper

Presented at the 133rd Convention  
2012 October 26–29 San Francisco, USA

*This Convention paper was selected based on a submitted abstract and 750-word precis that have been peer reviewed by at least two qualified anonymous reviewers. The complete manuscript was not peer reviewed. This convention paper has been reproduced from the author's advance manuscript without editing, corrections, or consideration by the Review Board. The AES takes no responsibility for the contents. Additional papers may be obtained by sending request and remittance to Audio Engineering Society, 60 East 42<sup>nd</sup> Street, New York, New York 10165-2520, USA; also see [www.aes.org](http://www.aes.org). All rights reserved. Reproduction of this paper, or any portion thereof, is not permitted without direct permission from the Journal of the Audio Engineering Society.*

---

## A Computational Acoustic Model of the Coupled Interior Architecture of Ancient Chavín

Regina E. Collecchia<sup>1</sup>, Miriam A. Kolar<sup>1</sup>, and Jonathan S. Abel<sup>1</sup>

<sup>1</sup>Center for Computer Research in Music and Acoustics, Stanford Univ., Stanford, CA, 94305, USA

Correspondence should be addressed to Regina E. Collecchia ([colleccr@ccrma.stanford.edu](mailto:colleccr@ccrma.stanford.edu))

### ABSTRACT

We present a computational acoustic model of the well-preserved interior architecture at the 3,000-year-old Andean ceremonial center at Chavín de Huántar, Perú. Our previous model prototype [Kolar *et al.* 2010] translated the acoustically coupled topology of Chavín gallery forms to a model based on digital waveguides (bi-directional by definition), representing passageways, connected through reverberant scattering junctions, representing the larger room-like areas. Our new approach treats all architectural units as “reverberant” digital waveguides, with scattering junctions at the discrete planes defining the unit boundaries. In this extensible and efficient lumped-element model, we combine architectural dimensional and material data with sparsely measured impulse responses to simulate multiple and circulating arrival paths between sound sources and listeners.

### 1. OVERVIEW

#### 1.1. Archaeoacoustic Research Context

Computational acoustic modeling of archaeological sites is a growing research area with the potential to provide new forms of evidence about the human past, while presenting new opportunities for applied acoustics. Such models document and preserve characteristics of ancient sound environments,

allow virtual reconstruction of the acoustics of damaged, destroyed, or implied site structures and materials, and can be developed into research tools for archaeological hypothesis testing, such as auralizations and sound transmission maps, in addition to the obvious utility for creating simulations for public interface applications. Our subject, the 3,000-year old Andean ceremonial center at Chavín de Huántar, Perú, is a site

dating to times of developing social hierarchy in the Andes. Human sensory experience is hypothesized to have been integral to ritual function [1] at this massive, multi-level temple complex built of stone block and earthen mortar. An exemplary subject for archaeoacoustic investigation, Chavín provides well-preserved enclosed interior architecture known as “galleries”, where acoustic measurements can be made [2] and auditory perception tested in on-site experiments [3], thus allowing for many aspects of acoustic models to be verified empirically. Site excavations have disinterred intact musical instruments, the *Strombus galeatus* marine shell aerophones known as “pututus”, that we simultaneously study for their potential as ancient sound generators [4], [5]. Our research team is developing an integrative archaeoacoustic methodology based on comparative studies of architectural and instrumental acoustics, combined with on-site auditory perceptual experimentation, to predict likely elements and interaction dynamics of ancient aural environments [6].

### 1.2. Acoustic Modeling for Chavín

Our target application for this computational acoustic modeling research is to create new archaeological tools for understanding sound transmission dynamics at Chavín, that can accept inputs of known or hypothesized sound sources, such as the artifact pututus or human voice. These models can be implemented as auralizations for psychoacoustic experimentation, in which the perceptual effects of sound source and environment dynamics can be systematically studied with controls to better understand the subjective link between human experience and its material evidence. The specification of a model to be used for psychoacoustically accurate simulations requires independent control over source and listener positions, directionality and orientation. Furthermore, it should be computationally inexpensive, and have real-time parameterization capabilities.

A survey of techniques used in modeling the acoustics of reverberant spaces (for example, [7], [8], [9], [10], [11]) did not provide us with a technology that would specifically address our subject, the narrow, labyrinthine, acoustically coupled interior architecture at Chavín. As a discipline, room acoustics simulation has focused

on larger, substantially uncoupled volumes: concert halls and performance venues, churches and cathedrals, modern commercial architecture, and other public gathering spaces. Computational approaches include 1) measured impulse response (IR) processing and playback, 2) approximation of wave propagation dynamics employing finite difference and finite element methods, 3) ray-based modeling (ray tracing and image-source methods), and 4) statistical modeling. These are often combined and hybridized to maximize strengths and minimize weaknesses (e.g., [7], [8], [10]), but all are restricted in terms of real-time viability. Methods based on IR measurement and processing are constrained in that they capture a closed set of dynamics between measured, fixed source and listener (S-L) positions, thus requiring extensive sampling to capture a representative range of S-L combinations within the space, with the accuracy of playback configurations limited to the measured configurations; this approach is logistically burdensome, computationally intensive, and by definition, incomplete. Though physical modeling approaches that reproduce wave propagation dynamics can do so with a high degree of accuracy, they are computationally expensive and inherently limited due to element resolution and the relationships between simulated wavelengths and room dimensions and geometries. Ray-based approaches model acoustic reflection paths, and are thus limited by algorithmic complexity, geometry dimensions and computational power, and vary in their handling of diffraction and diffusion. Statistical modeling methods can efficiently produce sound fields realistic in their density and overall temporal contour, but do not closely map characteristics of early sound unique to a particular space.

In considering the acoustic environment created by the architectural forms and layout of Chavín galleries, we saw an opportunity to abstract and recreate its unique character through a customized blend of techniques drawn from several computational acoustic modeling approaches, but elementally based on the digital waveguide, as discussed in §2.

### 1.3. Model Proposition

Our solution, initially proposed in [15] and

developed further here, is a lumped-element model that addresses the acoustically coupled layout and waveguide-like features of Chavín’s interior architecture; an exemplary gallery floorplan from the Laberintos Gallery is shown below.

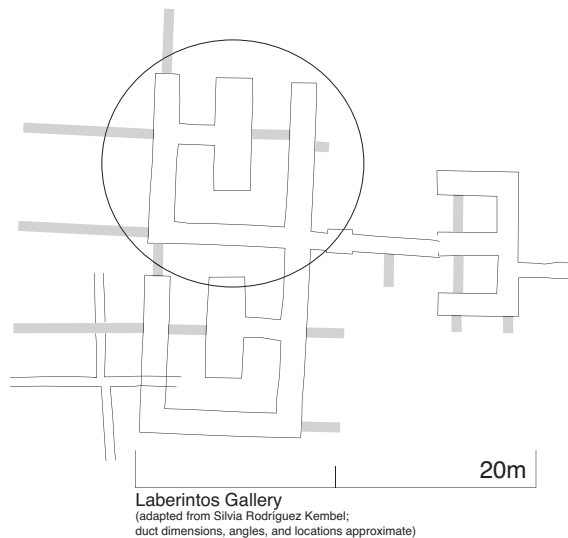


**Fig. 1:** The floorplan of the Laberintos Gallery at Chavín de Huántar. Our impulse response measurements come from the encircled section comprising six architectural units.

The narrow corridors and ducts (grey volumes in the above diagram) characteristic of Chavín gallery architecture can be computationally approximated using a physics-based synthesis framework, the digital waveguide [12], [13], [14]. The digital waveguide is a bi-directional delay line that models one-dimensional traveling wave propagation in acoustic systems. Seen as a modular network of interconnected ducts, the Chavín gallery topology readily translates to a computational acoustic modeling method called a digital waveguide network (DWN). In a DWN, bi-directional delay lines are interconnected by filter structures known as scattering junctions that emulate changes in energy distribution resulting from structural or other impedance changes.

The simplicity of a network built of one-dimensional digital waveguides provides computational efficiency, but cannot capture the complexity of the rapidly dense and diffuse echo sequence characteristic of gallery acoustics [2]. To emulate the diffuse early

sound field of Chavín galleries, we conceptualize a DWN built with reverberant waveguides that incorporate measured impulse response (IR) data [15], inspired by Spratt and Abel’s “Treeverb” [16] and earlier work by Abel, Huang, and Smith [17]. The specialized impulse response measurement method we developed to collect this data at Chavín is discussed in §4.

Digital waveguides (bi-directional delay lines) simulate the propagation of sound along gallery volumes, and are interconnected via scattering junctions (transmission filters), positioned where the volumes change cross-sectional area, turn corners, or otherwise intersect with areas that can functionally be considered separate waveguides. Measured impulse responses, sparsely sampled within and at the boundaries of the segmented architectural units that correspond to model waveguides, provide time-dependent frequency response data. Architectural dimensional data combined with features of the measured impulse responses are used to specify the filtering coefficients of the scattering junctions. Source and listener locations may be chosen interactively and, potentially, in real time, through specification of delays corresponding to physical location in spatial samples. The directional orientation of the source is resolved by our computational assumption that waves only propagate in two directions, such that the effective directionality of the sound can be determined by filters selected to approximate the radiation pattern of each specific source. The model can also incorporate binaural control for listener orientation using head-related impulse responses (HRIRs).

The result of the proposed approach is a computationally inexpensive model that directly translates architectural topology, captures salient acoustic features of the coupled spaces, and is extensible to other spaces whose architectural characteristics would benefit from similar handling. Research contributions are made in several areas. We advance knowledge of the sound environment at Chavín, a site whose importance to the human story is demonstrated by its near-millennium of ancient use and development; we also introduce a novel tool for research and public presentation in this archaeological application. In terms of spatial acoustics, we establish a computationally efficient

model for dealing with highly coupled architecture of small dimensions, as opposed to a single enclosed room of large volume such as a concert hall. Finally, we present an explicit method for specifying filters that accurately represents characteristics of measured impulse responses.

The advantages for our modeling application of using this lumped-element digital waveguide design versus that of the numerically based ray-tracing or finite difference time domain (FDTD) methods (see, e.g., [9], [10], [11]) follow from the physical characteristics of Chavín’s interior architecture. In §2, we connect its physical architecture to the architecture of our model. We present the model design in §3, and as an example, apply the method to the Laberintos Gallery of Chavín in §4. In §5, we evaluate our model. To conclude, we propose future research in §6.

## 2. MODEL ARCHITECTURE

To implement our modeling technique, we have chosen to simulate the acoustics of the west section of Upper Laberintos (“labyrinth”) Gallery, an exemplary case study for Chavín’s interior acoustics shown in Fig. 1. The interior architecture throughout the site is made up of narrow corridors, cells, and rooms, interconnected by horizontal “ventilation” ducts typically around 40 cm in diameter and of varied length. These spaces of different widths and heights intersect at orthogonal openings and comprise thousands of linear meters throughout the site. Gallery walls, typically 1 to 2 meters apart, are made of irregular, unfinished stone and clay mortar surfaces, with floors of reflective packed dirt and 1 to 2 meter-high ceilings of large smooth beams, often having stepped heights. Surface irregularities are on the order of wavelengths of sound from around 500 Hz to more than the limit of human hearing, thus making the rendering of an exact acoustic model computationally unreasonable.

These irregularities and corridor dimensions preclude standard ray-tracing as an appropriate method, which requires walls to be smooth, extensive planes that permit many wavelengths between parallel surfaces. Ray-tracing is based on specular reflection, in which the angle of incidence is equal to the angle of reflection, and therefore ignores

acoustic diffraction and diffusion, a broadband characteristic within extant gallery acoustics [2].

### 2.1. Signal Flow Architecture

Before we explore the measurements taken on site at Chavín de Huántar, we will relate an imagined floor plan to a signal flow diagram and identify the parts. In the diagram shown in Fig. 2, dotted lines separate architectural units into waveguides. We will call this Example A.

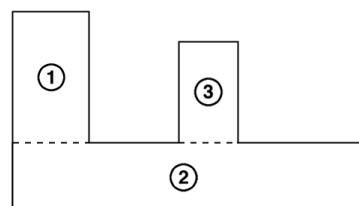


**Fig. 2:** Example A Floor Plan: an imagined network of three architectural units that meet at right angles.

In Example A, we have designated three architectural volumes that correspond to model *waveguides*, and refer to them with the notation  $G_1$ ,  $G_2$ , and  $G_3$ .

The dotted lines that divide these waveguides indicate the locations of lossless *scattering junctions*. We call these  $K_{12}$  and  $K_{23}$ , where  $K_{ij}$  connects waveguides  $G_i$  and  $G_j$  to one another.

Acoustic signals that flow through the space in Example A can be modeled with the signal flow diagram in Fig. 3.

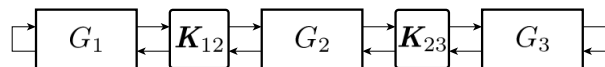


**Fig. 3:** Example A Signal Flow: signal flow for the three architectural units depicted in Fig. 2.

Note that we could have divided the waveguides in many different ways, another of which is shown in Fig. 4, which we refer to as Example B. The division of waveguides in Fig. 4 would correspond to a different signal flow diagram, depicted in Fig. 5.

Example B is not unlike modeling wave propagation inside a wind instrument, such as a flute or clarinet [18]. Impedance differences at the junction between the bore and the bell, and between the bore and the

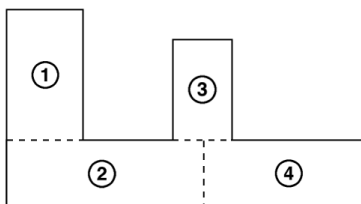


**Fig. 4:** Example B Floor Plan: another way of dividing the architectural units depicted in Fig. 2, into four waveguides this time. Dotted lines are once again representative of scattering junctions.

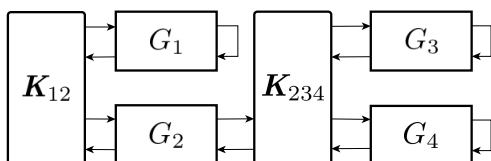


**Fig. 5:** Example B Signal Flow: represents the topology of the four architectural units depicted in Fig. 4.

tone holes, affect the propagation of waves along the instrument. At these impedance differences, energy from traveling waves either reflects back into the waveguide of their origination or transmits through to the next waveguide.

In §4, we apply this modeling method to the Chavín Laberintos Gallery, where we abstract an architectural area that corresponds to a circular network of waveguides and scattering junctions. We will now explain these elements in greater detail.

## 2.2. Waveguide Architecture

Each architectural volume (i.e., room, corridor, duct) represents a reverberant, bi-directional, digital waveguide in our model. Model waveguides are constructed with a digital delay line and filters that describe wave motion in the two directions. This delay is determined by the spatial length of the associated architectural unit, and is identical in either direction. The filters follow from measured impulse responses taken with a loudspeaker at one end of the architectural unit and a microphone at the other, as represented in Fig. 6.

Therefore, each waveguide  $G_i$  includes a forward-going filter  $X_i(z)$  and a backward-going filter  $Y_i(z)$ , each multiplied by the delay  $z^{-\tau_i}$  to compute the transfer functions with respect to direction. We

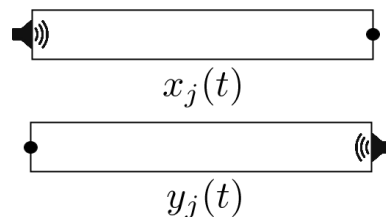


**Fig. 6:** Two impulse response measurements were taken per designated waveguide, with a microphone located at one boundary, and loudspeaker just outside the opposite end, then switched to capture both directions of traveling waves.

write it in the column vector

$$G_i(z) = \begin{bmatrix} X_i(z) \\ Y_i(z) \end{bmatrix} z^{-\tau_i}. \quad (1)$$

Its signal flow is given in greater detail in Fig. 7.

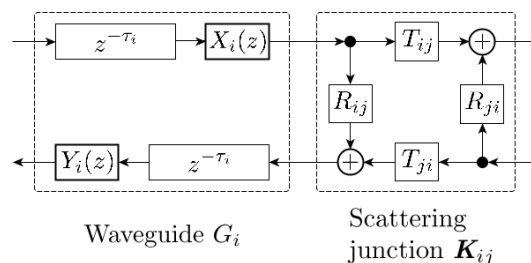


**Fig. 7:** A scattering junction  $K_{ij}$  connects waveguide  $G_i$  to  $G_j$  (not shown) and determines 4 coefficients:  $R_{ij}$ , the proportion of energy that reflects from waveguide  $G_i$  back into itself;  $R_{ji}$ , the proportion of energy that reflects from waveguide  $G_j$  back into itself;  $T_{ij}$ , the proportion of energy that leaves waveguide  $G_i$  and flows into  $G_j$ ; and  $T_{ji}$ , the proportion of energy that leaves waveguide  $G_j$  and flows into  $G_i$ . In the waveguides, we have a forward-going filter  $X_i(z)$  and a backward-going filter  $Y_i(z)$ , both associated with a time delay  $\tau_i$  related to the length of the waveguide.

By reducing architectural units to waveguides, our model becomes a one-dimensional approximation. A single impulse response measurement captures characteristics of acoustic propagation in either of two directions along the length of the waveguide. Since the waveguides represent gallery volumes, the propagation time/distance from one end to the other will be derived from the measured impulse response from each delineated architectural unit. Energy is dissipated within the waveguides, and the scattering junctions are lossless. Therefore, any energy arriving at the scattering junctions flows into the two adjacent waveguides.

### 2.3. Scattering Junction Architecture

Sound arriving at the scattering junction  $\mathbf{K}_{ij}$  from the waveguide  $G_i$  will interact with some portion of the sound being transmitted to the connected waveguide  $G_j$ , and some portion reflected back into the original waveguide  $G_i$ . Therefore, each scattering junction describes the acoustic interaction of waves approaching it from either side. We give it in matrix form as

$$\mathbf{K}_{ij} = \begin{bmatrix} R_{ij} & T_{ij} \\ T_{ji} & R_{ji} \end{bmatrix} \quad (2)$$

where  $R_{ij}$  refers to the amplitude scaling of a wave coming from waveguide  $G_i$  to reflect back into itself upon hitting the scattering junction;  $T_{ij}$  is the scaling applied to the signal transmitted to the waveguide  $G_j$ , and  $R_{ji}$  and  $T_{ji}$  are the reflection and transmission coefficients for waves that reach this scattering junction from waveguide  $G_j$ . The dimension of this matrix is determined by the number of conjoining waveguides—i.e., for  $N$  waveguides intersecting at a scattering junction, the matrix is  $N \times N$ .

This is a similar architecture to the Kelly-Lochbaum lumped-element model, which applies in one-dimensional cases to model waveguide-scattering junction interaction. The eigenvalues of the scattering junction matrices indicate to what degree energy is preserved in a given reverberant space, with an eigenvalue of 1 implying zero loss. Our scattering junctions are zero in volume and hence lossless, so we do expect our matrices to have eigenvalues of 1. However, we do not expect the geometry of Chavín to conform to the symmetric Kelly-Lochbaum model—i.e., for room  $A$  transmitting  $x$  proportion of its acoustic energy into an adjacent room  $B$ , room  $B$  may not transmit  $1-x$  proportion of its energy into room  $A$ —due to the approximations made in the dimensional reduction of our model. Therefore, our scattering junctions will preserve energy, but will not necessarily be of the Kelly-Lochbaum form.

### 2.4. Source-Listener Architecture

In our initial implementation of the model, we incorporate a listener (output) and a source (input) at desired locations in the model corresponding to actual places in the gallery, and use filters that

approximate antenna and radiation patterns. These filters can realistically simulate different source and listener orientations. As an example (Fig. 8), we make the waveguide unitary length, and depict a source and listener within the same waveguide, though their locations can be anywhere in the network.

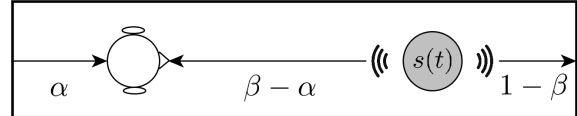


**Fig. 8:** A listener positioned at  $\alpha$  and source  $s(t)$  positioned at  $\beta$  along a waveguide of length 1. The distance between the source and listener is then  $\beta - \alpha$ . The source propagates sound waves to the left and right according to its radiation pattern. Right-going waves that transmit through the scattering junction at the right end of the waveguide travel through the rest of the network and arrive from behind the listener. Antenna and radiation patterns are not displayed.

We also show how sources may be input into the model at the spatial sample  $\beta$  along the  $j$ th waveguide,  $G_j$ , in Fig. 9.

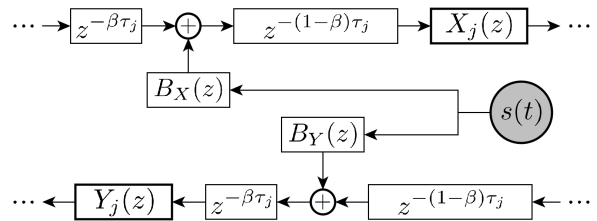


**Fig. 9:** A source  $s(t)$  affects the transfer function of a given waveguide by introducing a delay associated with its position along the waveguide and a radiation pattern in both the  $x$  and  $y$  directions. This delay is computed according to  $\beta$ , the source's position along the waveguide, where  $\beta = 0$  means the source is at the beginning of the waveguide and  $\beta = 1$  means the source is at the end. The radiation patterns are notated by  $B_X(z)$  and  $B_Y(z)$ .

Then, the output  $l(t)$  received by a listener is acquired by tapping out of the delay line at the spatial sample  $\alpha$  relating to the position of the listener. Antenna patterns may differ in the  $x$  and  $y$  directions, as noted in Fig. 10.

In summary, this signal flow model is topologically equivalent to the spatial architecture of a network of waveguide-like rooms exemplary of the interior

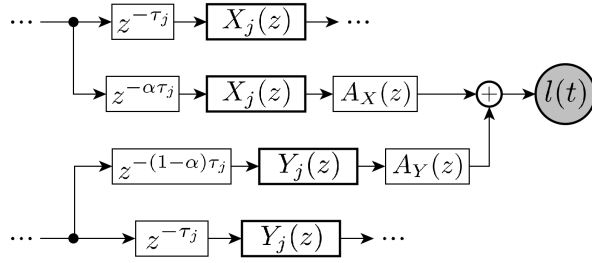


**Fig. 10:** The signal heard by a listener is determined by its location along the waveguide, denoted by the proportion  $\alpha$ , and the antenna pattern of the listener in both directions of the waveguide, given by  $A_X(z)$  and  $A_Y(z)$ . The spectra from these directions are summed and transformed to heed the signal  $l(t)$  heard by the listener.

architecture at Chavín. It represents the coupling of architectural units and the plausible recirculation of acoustic energy given appropriate dimensions and materials. We account for energy reflections and transmissions between waveguides at their boundaries with scattering junctions, and we allow for independent control of source and listener positions within the network by introducing appropriate delays and filters.

### 3. MODEL ELEMENT DESIGN

Following the discussion above, our model will characterize the flow of signals through a series of waveguides and scattering junctions. The waveguides are voluminous and lossy, and the scattering junctions are planar and lossless. Model topology relates directly to the layout of site architecture, and on-site impulse response measurements of the extant interior spaces at Chavín provide empirical data used in the model.

#### 3.1. Scattering Junction Filter Design

From Sabine [19], the total absorbing surface area of a room may be inferred from the volume, impulse response's energy density envelope, and the speed of sound.

We design our formulae for the reflection and transmission coefficients to be the ratio between this surface area implied by the reverberation time  $T_{60}$ , call it  $A_\alpha$ , and the measured surface area entryways

(modeled as connected waveguides in a room),  $A_{ij}$ ,

$$A_\alpha = 0.161 \frac{V}{T_{60}}, \quad (3)$$

where  $V$  represents the room volume. The reflection coefficients are then given by

$$R_{ij} = \sqrt{\frac{A_{ij}}{A_\alpha}}, \quad (4)$$

where  $A_\alpha$  refers to the total absorbing area of waveguide  $G_i$ . By the conservation of energy, the transmitted energy accounts for all of the energy that is not reflected, implying that

$$R_{ij}^2 + T_{ij}^2 = 1 \quad (5)$$

$$\Rightarrow T_{ij} = \sqrt{1 - R_{ij}^2}. \quad (6)$$

#### 3.2. Reverberant Waveguide Filter Design

We say that waveguide  $G_j$  is of length  $L_j$  and has an associated, maximum delay of  $\tau_j = L_j/c$  where  $c$  = the speed of sound in air;  $c$  is calibrated for measured impulse responses via recorded ambient conditions (temperature and humidity). The transfer function of the waveguide is calculated from the delay line depicted in Fig. 11, where the source is at the left termination of the waveguide and the microphone is at the right boundary.

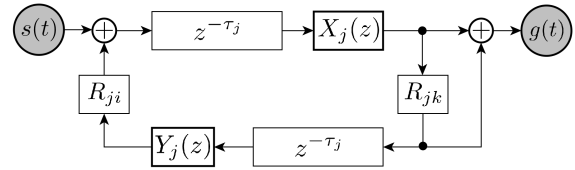


**Fig. 11:** Example signal flow representing a model waveguide unit, taken from impulse response measurements made with the corresponding architectural volume blocked at its boundaries. This diagram depicts a source  $s(t)$  which is input at the left termination of the waveguide and a microphone  $g$  placed at its right termination. The time delay  $\tau_j$  refers to the length of waveguide.

The transfer function of the  $j$ th waveguide in the  $x$ -direction is given by

$$G_X(z) = S(z) + H_{X_j}(z)R_{ji}H_{Y_j}(z)R_{jk}G(z) \quad (7)$$

where

$$H_{X_j}(z) = z^{-\tau_j}X_j(z), \quad (8)$$

$$H_{Y_j}(z) = z^{-\tau_j}Y_j(z). \quad (9)$$

Solving for  $G$ , we have

$$G_X(z) = \frac{H_{X_j}}{1 - R_{jk}R_{ji}H_{X_j}(z)H_{Y_j}(z)}. \quad (10)$$

Similarly, the transfer function in the  $y$ -direction is

$$G_Y(z) = \frac{H_{Y_j}}{1 - R_{ji}R_{jk}H_{Y_j}(z)H_{X_j}(z)} \quad (11)$$

when the source is positioned such that sound enters from the right of the waveguide and the microphone is switched to the left termination.

The impulse response measurement provides the desired transfer function, but includes contributions from energy reflected from the waveguide ends. These contributions have the effect of extending the reverberation time of the measured impulse response, so we suggest windowing the measured response by a decaying exponential. This will reduce the reverberation time to that noted during the first portion of the response, before the arrival of sound through the complimentary waveguide.

In addition to adjusting the decay time, the measured impulse response should be normalized for use in the model. We propose normalizing the impulse response to unit energy, and then scaling it by  $1 - (A_x + A_y)/A_\alpha$  to account for the energy lost to the materials in the space. It might be the case that some frequencies of the measured transfer function have gains greater than one even after normalization. In this case, we propose scaling by the inverse of the maximum gain before applying the factor  $1 - (A_x + A_y)/A_\alpha$ .

### 3.3. Source-Listener Interaction

The model's one-dimensional abstraction situates listeners and sources along the length of a waveguide. Since we assume that the pressure and velocity of sound waves are constant in a given slice of the waveguide along its width, a one-dimensional coordinate to position these objects is appropriate. More precise positioning and orientation details are handled by the filters specifying the listener's antenna pattern  $A(z)$  and the source's radiation pattern  $B(z)$ .

## 4. MODELING THE LABERINTOS GALLERY

In accordance with our rationale for translating architectural volumes into model units, we schematically and practically (given logistics of the on-site

measurement process) subdivided the Laberintos Gallery into 6 waveguides and 6 scattering junctions as shown in Fig. 12. Four measured impulse responses from waveguide  $G_1$  are plotted vertically in Fig. 13. The signal flow diagram corresponding to this network is shown in Fig. 14.

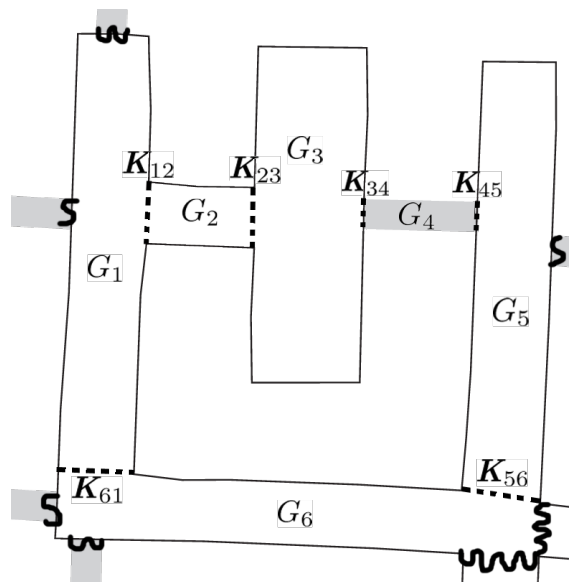


**Fig. 12:** We chose to divide the west section of Upper Laberintos Gallery into 6 waveguides, labeled with a  $G$ , and 6 scattering junctions, labeled with a  $K$  and dashed lines. Any volumes connected to this gallery section were blocked using tightly-packed sandbags or folded layers of heavy polyester-wool blankets, indicated in the diagram by wavy black lines.

On-site impulse responses were generated using the exponential sinusoidal sweep (ESS) method, reproduced via a Meyer MM-4XP loudspeaker located just outside the boundary of each designated waveguide, so that the test signal would pass through the entire unit. Four Countryman B6 omnidirectional microphones were positioned at the unit boundaries and at representative locations within each volume to record impulse responses in central locations. The filters  $X_i(z)$  and  $Y_i(z)$  follow from impulse response measurements taken at boundaries of each waveguide, as per Fig. 6. These are associated with a delay  $z^{\tau_i}$  (not depicted in Fig. 14) according to the spatial length of the waveguide, as in Fig. 7.

In the measurement process, entryways to each architectural volume—the boundaries of each model

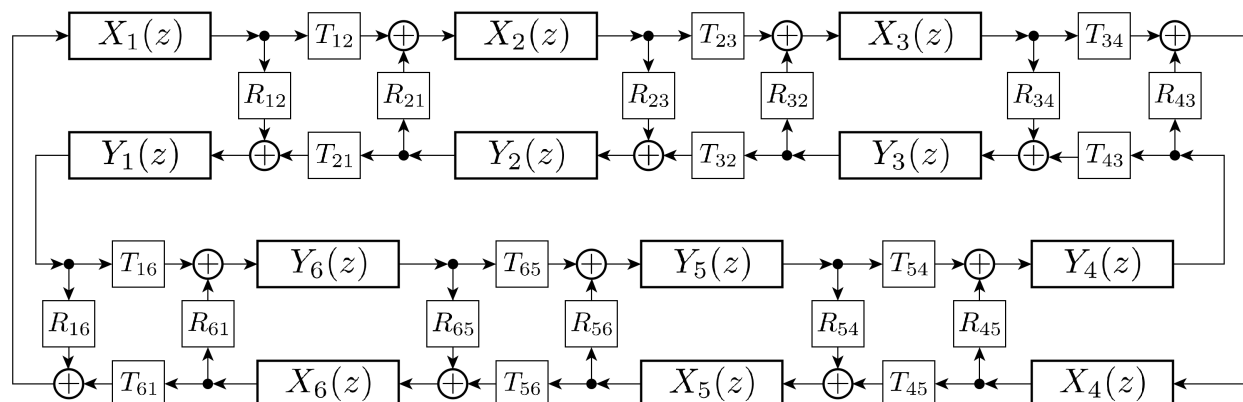


**Fig. 14:** The circular feedback delay network of corridors and ducts in our example implementation of the model for the west section of Upper Laberintos Gallery.

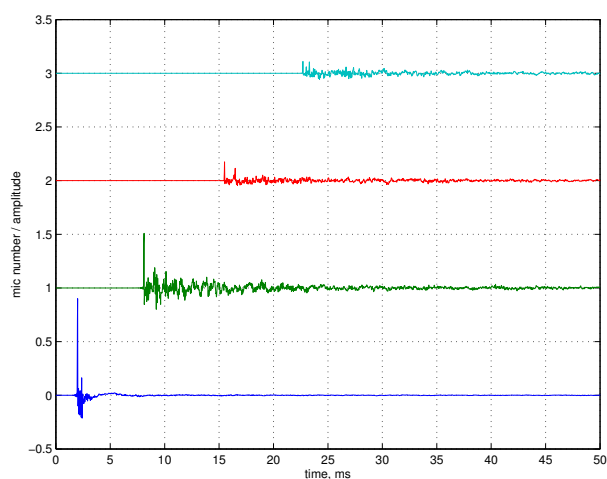


**Fig. 13:** Measured, normalized impulse responses recorded by four microphones placed sequentially in waveguide  $G_1$  of the Laberintos Gallery, in the  $x$  (clockwise) direction per model signal flow.

waveguide—were substantially blocked with several layers of folded polyester-wool blankets. The small (0.25m to 0.4m approximate diameter) ducts that exit Laberintos Gallery to other galleries and the building exterior were blocked with sandbags in order to capture data from selected architectural area. Blocking the terminations of each unit-designated-waveguide allows us to use the measured impulse responses to estimate reflection

coefficients for the boundary scattering junctions based on energy within each unit, and not on circulation through the network. Additional impulse measurements were made with unit boundaries open to provide data on the coupled architectural acoustic of the entire network. We use these to evaluate our model in the following section.

The measured dimensions of each waveguide are given in Table 1, as well as the ratio of the surface area of the packed dirt to the surface area  $A_\alpha$  of all absorptive materials in the given waveguide.

Wgd. ID	Dimensions of wgd. in meters	Proportion of dirt to $A_\alpha$
$G_1$	1.2w × 7.3l × 1.9h	0.1899
$G_2$	1.05w × 1.8l × 1.8h	0.1825
$G_3$	1.8w × 5.6l × 2.2h	0.1990
$G_4$	0.54w × 1.9l × 0.5-0.6h	0.0000
$G_5$	1.3w × 7.3l × 1.8h	0.2007
$G_6$	1.0w × 8.1l × 1.8h	0.1807

**Table 1:** The physical dimensions of each waveguide, which consist of packed earthen floors (except  $G_4$ , which is a narrow stone duct) and stone walls and ceilings. Since the packed earth is estimated to be more absorptive than the reflective walls and ceilings, a proportion of its surface area to the entire surface area of each waveguide is also given.

The surface areas of the scattering junctions are given in the following matrix, where the  $(i, j)$ th entry indicates the surface area between waveguide  $G_i$  and waveguide  $G_j$ . Therefore,  $A_{ij} = A_{ji}$ . Since many of the rooms do not directly interconnect,

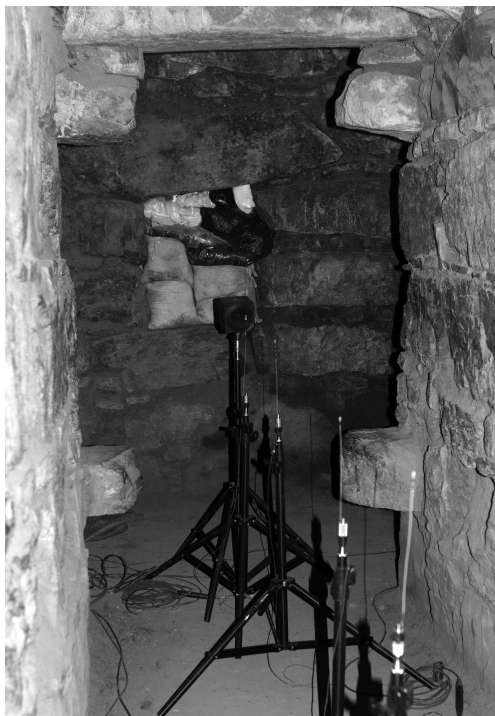


**Fig. 15:** On-site data collection in the Laberintos Gallery: impulse response measurements were made for each architectural volume that corresponds to a model unit. The exponential sinusoidal sweep test signal was produced via a Meyer MM-4XP loudspeaker located just outside the waveguide boundary, and the response recorded with four Countryman B6 omnidirectional microphones located within the volume. The shown measurement setup corresponds to waveguide  $G_2$  in our example implementation.

most of the elements will be 0. Significant digits were considered.

$$A_{ij} = \begin{bmatrix} 0 & 1.89 & 0 & 0 & 0 & 1.80 \\ 1.89 & 0 & 1.79 & 0 & 0 & 0 \\ 0 & 1.79 & 0 & 0.27 & 0 & 0 \\ 0 & 0 & 0.27 & 0 & 0.32 & 0 \\ 0 & 0 & 0 & 0.32 & 0 & 2.34 \\ 1.80 & 0 & 0 & 0 & 2.34 & 0 \end{bmatrix}$$

We computed  $T_{60}$  measurements for both types of impulse response measurements to support the calculation of our scattering junction coefficients (paired with the above matrix), and present these in Table 2. Since waveguide  $G_4$  has such a small cross-sectional area, it acts as an acoustic duct with a propagation delay and wall losses characterizing

the transfer function between the waveguide ends. Accordingly, the associated reverberation times are not tabulated. The reflection and transmission coefficients can be found by considering the radiation from a planar baffle.

Impulse resp. ID	$T_{60}$ without blankets	$T_{60}$ with blankets
$x_1(t)$	0.3043 s	0.2481 s
$y_1(t)$	0.3276 s	0.2409 s
$x_2(t)$	0.3740 s	0.1976 s
$y_2(t)$	0.3989 s	0.1887 s
$x_3(t)$	0.3606 s	0.3110 s
$y_3(t)$	0.3694 s	0.3570 s
$x_4(t)$	—	—
$y_4(t)$	—	—
$x_5(t)$	0.2964 s	0.2754 s
$y_5(t)$	0.2499 s	0.2834 s
$x_6(t)$	0.2642 s	0.2115 s
$y_6(t)$	0.3039 s	0.1974 s

**Table 2:** The  $T_{60}$  measurements corresponding to 2 measured impulse responses from each measured unit of Laberintos Gallery. This gives us the “characteristic decay time,”  $\tau$ , of each waveguide in the designated direction, and from these we can compute our reflection coefficients. Waveguide  $G_4$  is too acoustic duct-like to have a  $T_{60}$  time, so we compute its neighboring scattering junction coefficients using the radiation properties of a planar baffle.

## 5. MODEL EVALUATION

Additional measurements were taken to analyze the response of microphones located in all volumes of the selected network, without blocking unit terminations, thus capturing the acoustic coupling of the architectural acoustic system. In one such example measurement sequence, the loudspeaker was placed in the southeast corner of waveguide  $G_6$ . We changed the orientation of the speaker 17 times, and summed these impulse responses to simulate a hemispherically radiating source. In Fig. 16, we give as an example the impulse response recorded from a microphone located in the center of waveguide  $G_3$  in the open network. The modeled equivalent is shown in Fig. 17.

Via informal listening tests to compare these measured and modeled impulse responses, we conclude that this preliminary modeling method produces a somewhat “metallic” sound quality. We hypothesize that this is a result of room modes accentuated by repeated convolution.

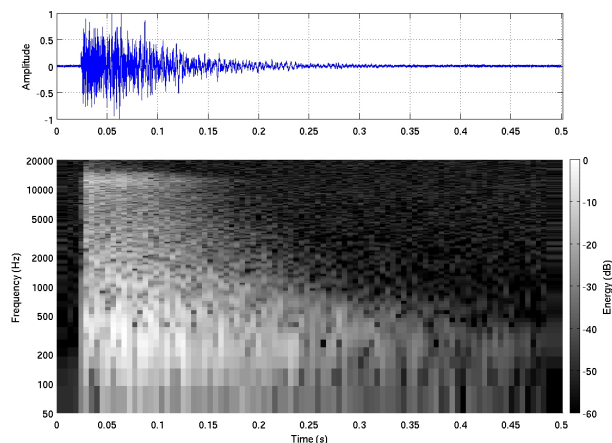


**Fig. 16:** The measured impulse response recorded by a microphone located in the center of waveguide  $G_3$  from a hemispherical source located in the southeast corner of waveguide  $G_6$ .

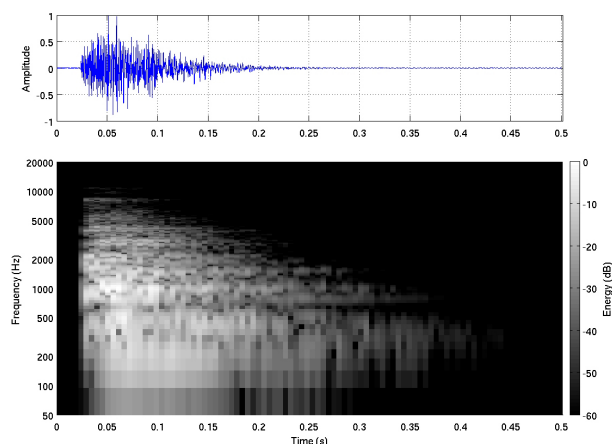


**Fig. 17:** The modeled impulse response corresponding to an impulse response recorded by a microphone located in the center of waveguide  $G_3$  from a hemispherical source located in the southeast corner of waveguide  $G_6$ .

## 6. FUTURE DEVELOPMENT

In future research, we plan to evaluate the perceptual validity of the model beyond informal listening tests through controlled psychoacoustic experimentation. Given psychoacoustic verification of a model of extant site architecture, we would consider the approach sufficiently robust to employ it in reconstructions of damaged or destroyed

structures. Archaeological hypotheses regarding differences in ancient structural conditions should be tested easily; for example, a straightforward change of model filter parameters would allow the model to simulate the acoustics of ancient Chavín galleries with wall surfaces of clay plaster, instead of the current rough stone and mortar.

Optimization for real-time implementation will be prioritized in the future to enable greater interactivity with dynamic source and listener positions.

In conclusion, this sparse and physics-based, modular acoustic model is a compelling solution for simulating the acoustics of Chavín galleries. It maps directly to gallery topologies and incorporates measured data to capture acoustic details in a flexible and efficient implementation. Because few field measurements are required to gather foundational data, this approach can significantly reduce the logistical demands of on-site data collection that other methods require. The lumped-element approach provides a flexible framework extensible to other architectural subjects having waveguide-like acoustic features, such as spaces with long corridors and multiple interconnected volumes.

## 7. ACKNOWLEDGMENTS

Ritesh Kolte collaborated with us to develop our model prototype in 2010, and David P. Berners provided helpful insights with respect to the acoustics of small rooms. We thank José Luis Cruzado for field support and documentation, and staff of the Peruvian Instituto Nacional de Cultura at the Monumento Nacional Chavín for other logistical assistance. Archeoacoustic research at Chavín de Huántar was initially funded by a grant from the Stanford Institute for Creativity and the Arts (SiCa), with continuing support through a Stanford Interdisciplinary Graduate Fellowship (SIGF) awarded to Miriam Kolar. Equipment sponsors include Countryman Associates, Inc. and Meyer Sound Labs.

## 8. REFERENCES

- [1] J. W. Rick, “The Evolution of Authority and Power at Chavín de Huántar, Perú,” *Archaeological Papers of the American Anthropological Association*, Vol. 14, 71-85, 2005.

- [2] J. S. Abel, J. W. Rick, P. Huang, M. A. Kolar, J. O. Smith, J. M. Chowning, "On the Acoustics of the Underground Galleries of Ancient Chavín de Huántar, Perú," presented at Acoustics '08, Paris, France, July 2008.
- [3] M. A. Kolar, "Archaeological Psychoacoustics at Chavín de Huántar, Perú." A dissertation to be submitted to the Department of Music and the Committee on Graduate Studies of Stanford University in Partial Fulfillment of the Requirements for the Degree of Doctor of Philosophy (in press).
- [4] P. R. Cook, J. S. Abel, M. A. Kolar, P. Huang, Jyri Huopaniemi, John W. Rick, Chris Chafe, John M. Chowning, "Acoustic Analysis of the Chavín Pututus (*Strombus galeatus* marine shell trumpets)." Invited paper presented at the 2nd Pan American/Iberian Meeting on Acoustics, Cancún, México, November 2010.
- [5] M. A. Kolar, P. R. Cook, J. S. Abel, J. W. Rick, "Acoustics, Architecture and Instruments in Ancient Chavín de Huántar, Perú," presented at XII Congress ICTM Study Group for Music Archaeology, Sound and Ritual: Bridging Material and Living Cultures, University of Valladolid, Spain, September 2011.
- [6] M. A. Kolar, J. W. Rick, P. R. Cook, J. S. Abel, "Ancient Pututus Contextualized: Integrative Archaeoacoustics at Chavín de Huántar, Perú," Studies in Pre-Columbian Music Archaeology - Estudios en Arqueomusicología Precolombina, Vol. 1. Edited by Matthias Stöckli and Arnd Adje Both. Berlin, 2012 (in press).
- [7] M. Karjalainen, P. Huang, J. O. Smith III, "Digital Waveguide Networks for Room Response Modeling and Synthesis," Convention Paper 6394, presented at the 118th Audio Engineering Convention, Barcelona, Spain, 28-31 May 2005.
- [8] L. Savioja, J. Huopaniemi, T. Lokki, R. Väänänen, "Creating Interactive Virtual Acoustic Environments." *Journal of the Audio Engineering Society of America*, 47 (2), September 1999.
- [9] T. Funkhouser, N. Tsingos, I. Carlbom, G. Elko, M. Sondhi, J. E. West, G. Pingali, P. Min, A. Ngan, "A Beam Tracing Method for Interactive Architectural Acoustics," *Journal of the Acoustical Society of America*, 115 (2): 739-756, February 2004.
- [10] D. T. Murphy, M. Beeson, S. Shelley, A. Southern, A. Moore, "Hybrid Room Impulse Response: Synthesis in Digital Waveguide Mesh Based Room Acoustics Simulation," *Proceedings of the 11th International Conference on Digital Audio Effects (DAFx-08)*, pp. 129-136, Espoo, Finland, September 2008.
- [11] E. D. Sena, H. Hacihabiboglu, Z. Cvetković, "Scattering Delay Network: an Interactive Reverberator for Computer Games," presented at the Audio Engineering Society 41st International Conference, London, UK, 2-4 February 2011.
- [12] J. O. Smith, "A New Approach to Digital Reverberation using Closed Waveguide Networks," *Proceedings of the 1985 International Computer Music Conference*, Burnaby, B.C., Canada, pp. 47-53, 1985.
- [13] J. O. Smith, "Physical modeling using digital waveguides," *Computer Music Journal*, 16 (4): 74-87, 1992.
- [14] J. O. Smith, "Principles of Digital Waveguide Models of Musical Instruments," *The International Series in Engineering and Computer Science*, 1, Volume 437, Applications of Digital Signal Processing to Audio and Acoustics, pp. 417-466, Springer, 1998.
- [15] M. A. Kolar, J. S. Abel, R. Kolte, P. Huang, J. W. Rick, J. O. Smith, C. Chafe, "A Modular Computational Acoustic Model of Ancient Chavín de Huántar, Perú," presented at the 2nd Pan American/Iberian Meeting on Acoustics, Cancún, México, November 2010.
- [16] K. Spratt, J. S. Abel, "A Digital Reverberator Modeled after the Scattering of Acoustic Waves by Trees in a Forest," presented at the Audio Engineering Society 125th Convention, San Francisco, 2-5 October 2008.
- [17] J. S. Abel, P. Huang, J. O. Smith III, "Waveguide Mesh Reverberator with Internal Decay and Diffusion Structures," Convention Paper 7194, presented at the Audio Engineering Society 123rd Convention, New York, NY, 5-8 October 2007.
- [18] T. Smyth, J. S. Abel, "Modeling and Measurement of Wind Instrument Bores," presented at the 19th International Congress on Acoustics, Madrid, 2-7 September 2007.
- [19] W. C. Sabine, *Collected Papers on Acoustics*. Cambridge: Harvard University Press, 1923.